



Imaging of normal lung, liver and parotid gland function for radiotherapy

Mike Partridge, Tokihiro Yamamoto, Cai Grau, Morten Høyer & Ludvig Paul Muren

To cite this article: Mike Partridge, Tokihiro Yamamoto, Cai Grau, Morten Høyer & Ludvig Paul Muren (2010) Imaging of normal lung, liver and parotid gland function for radiotherapy, Acta Oncologica, 49:7, 997-1011, DOI: [10.3109/0284186X.2010.504735](https://doi.org/10.3109/0284186X.2010.504735)

To link to this article: <https://doi.org/10.3109/0284186X.2010.504735>



Published online: 13 Sep 2010.



Submit your article to this journal [↗](#)



Article views: 1770



View related articles [↗](#)



Citing articles: 4 View citing articles [↗](#)

REVIEW ARTICLE

Imaging of normal lung, liver and parotid gland function for radiotherapy

MIKE PARTRIDGE¹, TOKIHIRO YAMAMOTO², CAI GRAU³, MORTEN HØYER³
& LUDVIG PAUL MUREN³

¹The Institute of Cancer Research, Sutton, UK, ²Stanford University School of Medicine, Stanford, CA, USA and ³Aarhus University Hospital, Aarhus, Denmark

Abstract

There is growing clinical evidence that functional imaging is useful for target volume definition and early assessment of tumour response to external beam radiotherapy. A subject that has perhaps received less attention, but is no less promising, is the application of functional imaging to the prediction or measurement of radiation adverse effects in normal tissues. In this manuscript, we review the current published literature describing the use of positron emission tomography (PET), four-dimensional computed tomography (4D-CT), single photon emission computed tomography (SPECT) and magnetic resonance imaging (MRI) to study normal tissue function in the context of radiotherapy to the lung, liver and head & neck. Published results to date demonstrate that functional imaging can be used to preferentially avoid normal tissues not easily identifiable on solely anatomical images. It is also a potentially very powerful tool for the early detection of radiotherapy-induced normal tissue adverse effects and could provide valuable data for building predictive models of outcome. However, one of the major challenges to building useful predictive models is that, to date, there are very little data available with combined images of normal function, 3D delivered radiation dose and clinical outcomes. Prospective data collection through well-constructed studies which use established morbidity scores is clearly a priority if significant progress is to be made in this area.

The introduction of functional imaging, such as positron emission tomography (PET), dynamic magnetic resonance imaging (MRI), and single photon emission computed tomography (SPECT), into radiotherapy (RT) planning and evaluation is one of the major current research areas in our field [1–3]. These imaging techniques have been developed to portray biological characteristics of tissue. For tumours, they can visualise important hallmarks of cancer, such as blood perfusion/oxygenation and energy metabolism [4]. Since the radiosensitivity of tumour cells strongly depends on these factors, there is a broad spectrum of investigations on-going to explore whether functional imaging can be used to prescribe, in greater detail than today, dose to the parts of the tumour with radioresistant (e.g. oxygen-deficient) cells. For normal tissues, on the other hand, functional imaging has received far less attention but is also likely to play an important role [5].

These imaging techniques could provide 3D maps of normal tissue function, which in turn could be used to guide the deposition of radiation to parts of an organ where baseline function is reduced or absent. A premise of this research area is the observation that vascular damage is a major component in the development of normal tissue adverse effects after RT, in combination with the fact that change in tissue vascularity is one of the main parameters that can be quantified with a number of the functional imaging techniques [6–11].

In current RT planning for a number of tumour sites, estimation of the potential risks of normal tissue irradiation is based on the assumption of spatially uniform tissue function. However, there is evidence from a number of the normal tissues that are important organs at risk in RT – e.g. lung, liver and brain tissue – that the functional sub-units that contribute to whole organ function are not uniformly distributed

throughout the volume of the organ [12]. In addition, it is starting to be appreciated that patients referred to RT present with considerable spatial variations in organ function, e.g. in the lungs, depending on the impact of the tumour growth and the patients' co-morbidities. The advent of recent RT delivery techniques, to some extent with intensity-modulated RT (IMRT) and more explicitly with arc-therapy techniques (where the whole gantry-angle space is used) [13], opens new possibilities for directing radiation beams along carefully selected paths which account for the spatial patterns of normal tissue function.

The use of normal tissue functional imaging could also have considerable impact on our ability to predict normal tissue adverse effects, with implications for both patient selection and individual RT dose prescriptions [14]. The assumption of spatially uniform function has also been the basis for the studies of the relations between dose/volume parameters of normal tissues and their response. In parallel with the potential for improved RT planning based on functional imaging described above, a similar potential appears for RT evaluation and risk predictions. Besides, with the development of '3D morbidity' measures appearing with functional imaging (as opposed to today's binary or scalar morbidity measures), a related original area of research lies in the development of statistical models of the relations between 3D morbidity and 3D dose.

In this manuscript, we review the current published literature describing the application of functional imaging to the prediction or measurement of radiation adverse effect in normal tissues during external beam RT. We discuss published strategies and potential future applications for incorporating this information on normal tissue function into the RT planning and evaluation process, with specific reference to the use of PET, SPECT, four-dimensional x-ray computed tomography (4D-CT) and MRI to study normal tissue function in RT involving the lung, liver and the parotid glands.

Methodology and scope

The work described in this article was identified using MEDLINE and PubMed searches, carried out using the terms "functional imaging", "treatment planning" and "radiotherapy". Suitable articles were retrieved for full critical appraisal. Back-tracking was performed from reference lists of the articles found using this search strategy.

For a given functional imaging technique to be usefully applied to normal tissue definition in RT planning or predictions of normal tissue response to RT (for example, by inclusion in functional normal

tissue complication probability models), there are in general three main criteria that should be satisfied:

1. The imaging technique should be sufficiently well developed that it delivers reliable measures of *relevant* organ function; ideally with known and good quantitative accuracy. The gold-standard for this would be clinical validation of the technique against histopathological or other relevant data.
2. To benefit from imaging the spatial distribution of function, it should be likely that heterogeneity of function will exist, either due to the structure of the organ, or as a result of disease. The organ should also be capable of continuing to function to some degree when one part of it has been damaged or occluded (i.e. it exhibits a degree of "parallel" functional behaviour).
3. The geometry of the target volume and normal tissues should present a challenge for treatment planning. Normal tissues that "wrap around" the target (such as normal lung and liver around lung and liver tumours respectively) are clear examples of this: it is inevitable in such cases that the normal tissues will receive some radiation dose. With the addition of functional imaging, the dose to the "best-functioning" portions of the tissue can be minimised by optimisation of beam directions and the use of IMRT, or optimum arc lengths and trajectories.

Three anatomical sites where the above three prerequisites clearly seem to be fulfilled are the lung, liver and parotid glands. This is by no means an exhaustive list, but we have chosen to concentrate on these three areas for the remainder of this review. They are discussed in turn below.

Imaging of lung function

Radiation pneumonitis is usually the main dose-limiting end-point in RT for non-small cell lung cancer (NSCLC) and the parameters V_{20} (the volume of lung receiving >20 Gy) and mean lung dose are commonly used as predictors of this [15]. However, reduction of pulmonary function can also be a complication of thoracic RT, and may seriously impact quality of life. Dose-volume statistics alone are not reliable predictors of radiation-induced change in pulmonary function, particularly in patients with co-existing cardio-pulmonary disease. The use of functional imaging as a method for quantifying pre-RT pulmonary function, and potentially minimising radiation damage to healthy lung, is therefore of significant current interest.

^{99m}Tc MAA SPECT

The first demonstration that ^{99m}Tc-labelled macro-aggregated albumin (MAA) SPECT potentially could be used to design “optimal” lung radiation treatments came from Marks et al. at Duke University Medical Centre, Durham, USA [16]. In a trial of 18 patients immobilised and SPECT scanned in the RT treatment position, post-RT scans saw reductions in regional lung function one to six months post treatment for regions receiving >40 Gy. It was therefore suggested that MAA SPECT could be used to assess the potential effect of RT on regional lung function, although at that time the regional dose-response relationship was unknown. The incorporation of functional information into traditional dose-volume histogram (DVH)-based dose-response models required the introduction of the concept of the “functional” DVH or fDVH [17] (also referred to as a DVfH by some authors). The Duke University group went on to assess the use of SPECT to predict the pulmonary consequences of thoracic RT and found that such SPECT-derived fDVHs did not appear to add predictive value over and above straight-forward NTCP models [12]. They concluded that both dose-volume and pre-RT pulmonary function tests are important, due to the highly variable baseline function seen in this population.

Interestingly, it has been shown that DVH reduction using either empirical [18] or parallel functional sub-unit based models [19] are mathematically identical, provided that the local dose-effect relationship obeys a power law in the clinically relevant dose range [20]. It was demonstrated that the local dose-effect for lung using ventilation/perfusion SPECT could be described using a power law relation with n in the range 0.8 to 0.9 (which was in agreement with the typically cited value of $n = 0.87$). Furthermore, mean lung dose was also shown to give very similar predictive results to the two DVH reduction methods. Later work by Nioutsikou [14] extended the Lyman [21] model to explicitly include function with the familiar organ parameters n , m , and TD_{50} replaced by parameters referring solely to the part of the organ defined as functional: n_f , m_f and TD_{50f} . By exploring the parameter space of this equation it was shown that the addition of functional information has most benefit for organs with a large volume effect and large focal regions of dysfunction. Again functional NTCP predictions were in agreement with those from mean perfusion-weighted lung dose.

In an observational trial of 104 patients with pre-RT SPECT scans, the Duke University group showed that SPECT provided potentially useful information due to detection of hypoperfused regions of lung in 48% of cases. Using a relatively straight-forward AP-PA treatment technique, plans could be usefully

modified in 11% of cases [22]. A more sophisticated planning technique employing perfusion-weighted optimisation of a 7-field conformal plan was reported by Seppenwoolde et al. [23], but it was again shown that improved treatment plans could only be produced for patients with large pre-treatment perfusion defects. This was further emphasised by Christian et al. [24], who nicely demonstrated the clinical feasibility of accurate co-registration of SPECT and CT, but again only showed a reduction in fV_{20} (the volume of SPECT-functioning lung receiving >20 Gy) in patients with focal perfusion deficit, for conformal treatment planning (Figure 1).

The use of intensity-modulated RT (IMRT) to preferentially avoid well-perfused lung was shown in a small study by McGuire et al. (five patients) [12]. IMRT was shown to be beneficial over conformal planning, with more favourable dose-function histograms generated for all patients and a reduction in fV_{20} by $13.6 \pm 5.2\%$ with IMRT compared to conformal plans [25]. A similar study reported by Lavrenkov et al. showed statistically significant improvements in the ratio of target coverage to functional lung avoidance (PTV_{90}/fV_{20}) when using IMRT compared to 3D conformal planning for stage

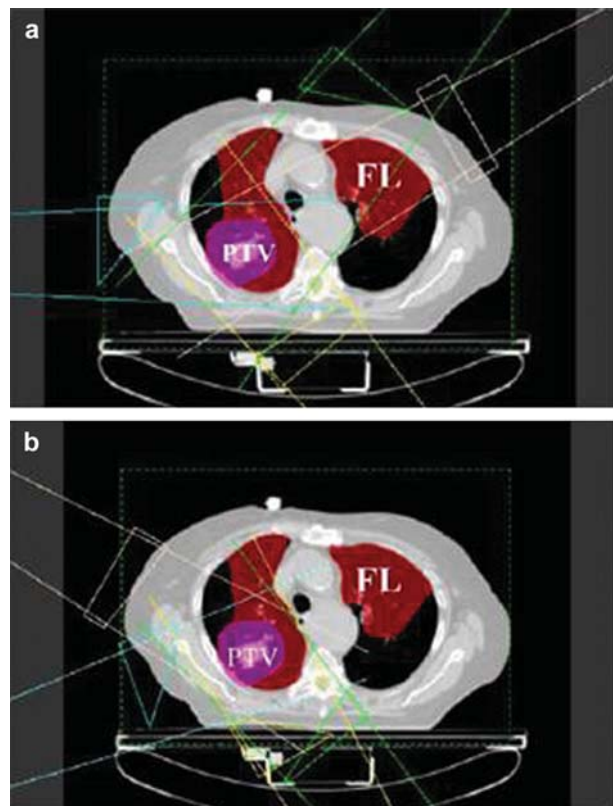


Figure 1. Illustration of the influence of functional imaging on RT planning. Panel a) shows a coplanar plan where functional information was not used. In panel b) functioning lung was preferentially avoided when selecting coplanar beam directions. From Christian et al. [24].

IIIA and IIIB disease. Interestingly, no improvement was seen for early stage patients (stage I and II), concluding that IMRT has no advantage over conformal RT in patients with more localised disease or with localised perfusion deficit [26,27].

The underlying hypothesis of all of the above work is that it is clinically beneficial to spare as much functioning lung as possible during RT, subject to adequate target coverage. Although this may seem intuitively obvious, the experimental and clinical evidence behind this hypothesis has only recently begun to emerge. Van Luijk et al. [28] show experimental evidence that radiation-induced pulmonary function correlates with structural changes in rat lung in the absence of confounding cardiac toxicity caused by coronary irradiation. In clinical practice little structural change is seen on CT for doses below 40 Gy, but a gradual dose-response has been reported for ventilation and perfusion SPECT [8].

Recent results from Duke University do show that, for a cohort of 81 patients with concurrent post-RT SPECT, there is a weak quantitative association between clinically measured pulmonary function tests and SPECT-defined lung perfusion [29]. Measured changes in SPECT-defined perfusion as a result of RT have also shown that “thoracic RT causes dose-dependent reductions in regional lung perfusion that progress up to about 18 months post-RT and persist thereafter. There appears to be similar dose response for healthy parts of the lungs at different locations” [30]. It has therefore been shown that there is an association between integrated response and whole lung function, albeit with relatively low correlation coefficients. Additional work is needed to better relate regional injury and changes in whole lung function.

³He-MRI

Radioisotope imaging is not the only method for quantifying lung function. Ireland et al. at the University of Sheffield, UK, have very nicely demonstrated the use of hyperpolarised ³He-MRI for visualising ventilation. In a feasibility study of six patients with NSCLC, they were able to demonstrate statistically significant reductions in V_{20} and fV_{20} when using IMRT to avoid regions of high ³He-MR signal [31]. In a follow-up study on the same patient population, very similar reductions in V_{20} and fV_{20} were obtained for both SPECT-based and ³He-MR-based functional avoidance [32]. Work by the same group found CT to ³He-MR registration accuracy could be improved by using breath-hold rather than free-breathing CT [33].

Four-dimensional (4D) computed tomography (CT)

Pulmonary ventilation images can also be created from 4D-CT. A novel two-step technique has been described using (1) a spatial voxel-wise mapping of different respiratory phases of 4D-CT images using deformable image registration, and (2) quantitative analysis of the resultant displacement vector field for computing a ventilation metric (Figure 2). Guerrero et al. at M. D. Anderson Cancer Centre originally developed this method using paired breath-hold CT images [34]. They used deformable image registration to map the peak-exhale CT image to the peak-inhale image, and calculated the change in the air fraction per voxel as a metric of regional ventilation based on the theory proposed by Simon [35]. To date several investigators have applied this method to 4D-CT images with some modifications, and currently at least four groups have been investigating this technique, including M. D. Anderson [34,36,37], the

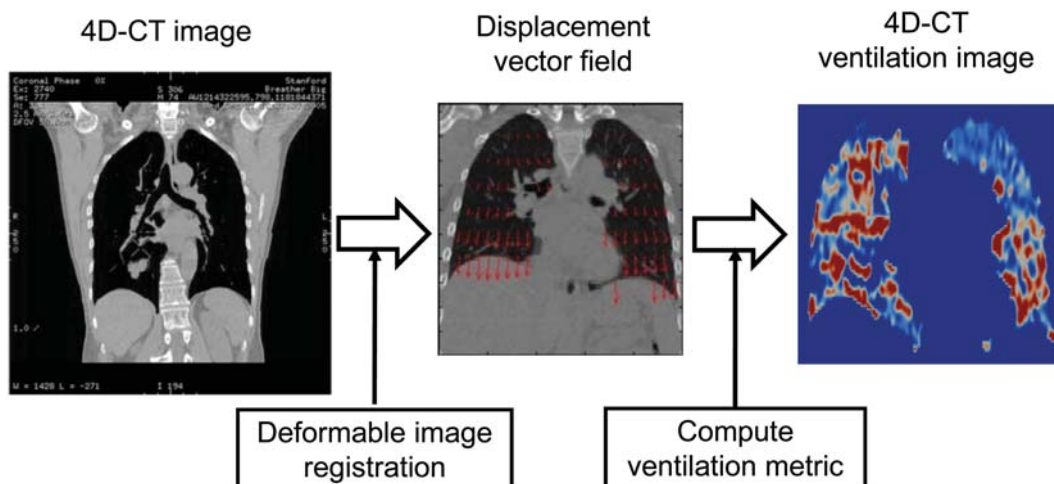


Figure 2. Schematic diagram for creating a 4D-CT ventilation image through deformable image registration and quantitative analysis of the resultant displacement vector field for computing the ventilation metric.

University of Iowa [38], Henry Ford [39], and a collaborative group between Stanford University and Philips Research Europe [40–42]. In contrast to the other techniques (e.g. MAA SPECT, ^3He -MRI and Xe-CT), the 4D-CT ventilation can be considered as ‘free’ information for lung cancer radiotherapy patients, because 4D-CT scans are in routine use for these patients in many centres, and ventilation computation involves only image processing (i.e. deformable image registration) and analysis. Moreover, 4D-CT ventilation imaging is faster, has higher resolution, and/or is more widely accessible from radiotherapy centres than the other techniques.

Although 4D-CT ventilation imaging has several advantages over the other techniques, its physiological accuracy has not been validated. The global accuracy has been investigated by comparing the changes in the total lung volume calculated with the 4D-CT ventilation to those measured with the segmented lung volumes from 4D-CT images, and found to be promising [34,36,42]. Guerrero et al. demonstrated a strong correlation coefficient ($r = 0.985$) between the calculated and measured volume changes [36]. Reinhardt et al. at the University of Iowa compared the mean 4D-CT ventilation and the mean Xe-CT ventilation in the 4 mm thick subregions spaced along the anterior-posterior direction for five anaesthetised sheep, and demonstrated reasonably strong correlations (average, $r^2 = 0.73$) [38]. These studies indicate the potential of 4D-CT ventilation imaging; however more thorough validation of regional and physiological accuracy in patients is necessary, especially given that there are various deformable image registration algorithms and two ventilation metrics that have been and could be used for 4D-CT ventilation computation [34,36,38,42–45]. Figure 3 shows example 4D-CT ventilation images derived using the different combinations of two deformable image registration algorithms: surface-based registration [46,47] and non-parametric volume-based registration [42], and two ventilation metrics: Hounsfield

unit (HU)-change and Jacobian determinant of deformation. Different registration algorithms and metrics yield spatially variant 4D-CT ventilation images. Recently the Stanford/Philips group evaluated 4D-CT ventilation imaging by correlating ventilation with pulmonary emphysema for 12 patients who had emphysematous lung regions, which was the first study to investigate a physiological aspect of 4D-CT ventilation imaging in patients [41]. There is destruction of alveolar septa in emphysema, leading to decreased elastic recoil of the alveoli and less radial traction. Thus emphysematous lung regions are expected to be poorly ventilated. They showed that the HU-based 4D-CT ventilation was significantly lower in emphysematous regions than in non-emphysematous regions ($p < 0.001$), however the Jacobian-based ventilation showed a non-significant difference ($p = 0.218$). This study indicates a potential of 4D-CT ventilation imaging with the HU metric to achieve the high physiological accuracy. A further study is still needed to confirm this result, e.g. validation against SPECT ventilation scans.

Four-dimensional ventilation images have also been used for lung functional avoidance in radiotherapy treatment planning, as with SPECT and ^3He -MR images as described above. For the first time, Yaremko et al. at M. D. Anderson investigated 4D-CT ventilation image-guided IMRT treatment planning for 21 Stage III NSCLC patients [37]. They demonstrated a significant reduction in the mean dose to the 90th percentile functional volume (the 10% of the lung volume with the highest ventilation) of 2.9 Gy ($p < 0.001$). Recently, Yamamoto et al. at Stanford also quantified the dosimetric impact of 4D-CT ventilation image-guided planning with volumetric-modulated arc therapy (VMAT) in addition to IMRT for 15 Stage I–III NSCLC patients [40]. Figure 4 shows the isodose distributions for anatomical and functional VMAT plans for one example patient. Of particular note are the 20 and 40 Gy isodose curves, which are distorted to spare

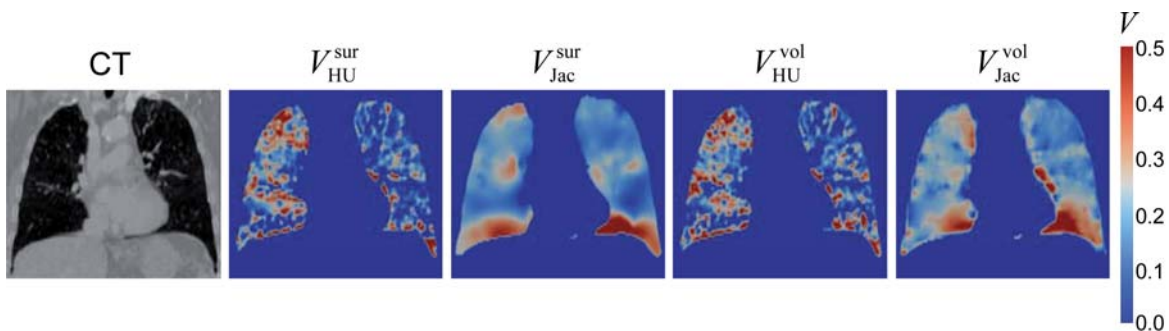


Figure 3. Example coronal images at the same level of peak-exhale CT and 4D-CT ventilation derived from the different combinations of two deformable image registration algorithms: surface-based registration and non-parametric volume-based registration, and two ventilation metrics: Hounsfield unit (HU)-change and Jacobian determinant of deformation.

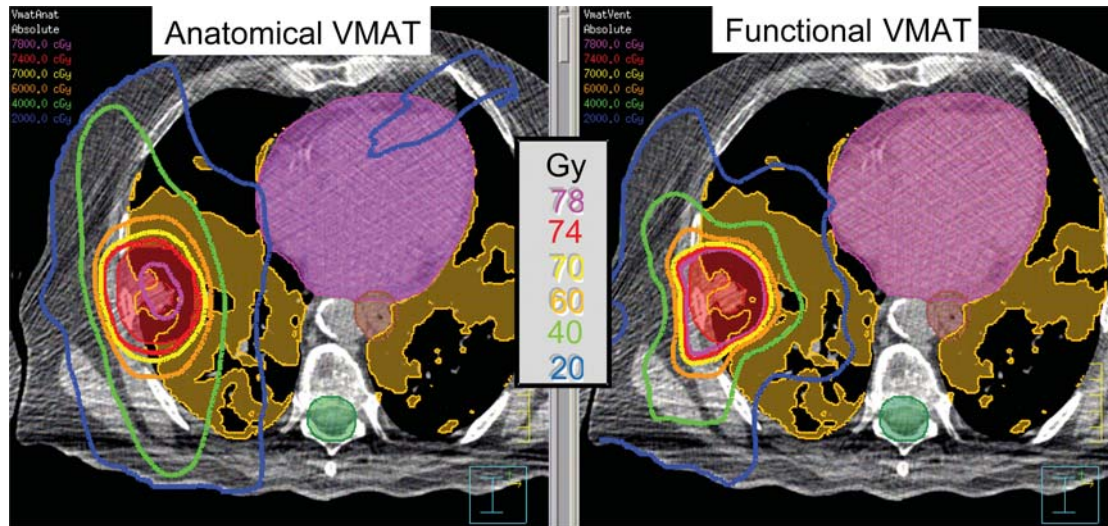


Figure 4. Example isodose distributions of anatomical and functional VMAT plans. Functional VMAT spared the highly-functional lung, and anatomical VMAT treated the lungs as uniformly functional. Highly-functional lung regions are shaded orange; PTV red; spinal cord planning organ-at-risk volume (PRV) green; oesophagus PRV brown and heart pink.

highly-functional lung, significantly reducing mean dose to the highly-functional lung by 1.8 Gy ($p < 0.001$) for IMRT, and 2.0 Gy for VMAT ($p < 0.001$). Also, significantly larger reductions were observed for patients with a larger amount of highly-functional lung adjacent to the PTV than those with a smaller amount (e.g. mean dose, 3.4 Gy vs. 0.1 Gy for VMAT, $p = 0.004$). These findings indicate the potential of 4D-CT ventilation image-guided planning in functional lung avoidance for both IMRT and VMAT.

Although in this review we have concentrated on pre-treatment imaging, functional imaging can also be used to assess normal tissue damage in the lung. Both PET and SPECT have been shown to be useful for imaging pneumonitis [48]. CT has also been shown to be useful for assessing post-RT fibrosis [49] and, despite strong patient-specific variations in fibrosis volumes being observed, local Monte Carlo dose was seen to correlate with the probability of radiation-induced fibrosis and could form a sound basis for future systematic numerical studies.

Summary

The clinical feasibility of using images of lung function in RT planning has clearly been demonstrated. It has been shown that statistically significant reductions in dose to functioning lung can be achieved for the small percentage of patients with large focal functional deficits or with a large amount of functioning lung adjacent to the PTV. The use of IMRT or modulated arc therapy techniques to preferentially avoid functioning lung has also been shown to further improve dose distributions, particularly for later stage

(IIIA and IIIB) disease. Provided that it can be properly validated, 4D-CT is emerging as a very attractive method for measuring lung ventilation “for free”. However, accurate knowledge of the dose-response of lung tissue as a function of perfusion is still unclear. Clinical and experimental evidence has recently begun to emerge showing that dose-dependent reductions in regional lung perfusion can be observed and a weak association between integrated response and whole lung function has been reported. Before widespread clinical implementation of such a technique, further research – ideally in the form of prospective clinical trials – is required to allow better selection of which patients would gain most clinical benefit from image-guided functional-lung avoidance.

Imaging of liver function

There is growing interest in the use of RT in treatment of liver tumours. Conventional techniques as well as hypofractionated stereotactic body RT are now frequently used in the treatment of primary cancers and metastases of the liver. In many centres these techniques have become an established part of multidisciplinary team services, which includes hepatobiliary surgery and non-surgical ablative modalities.

Anatomically the liver consists of eight segments, each supplied with blood from the portal vein and the hepatic artery with drainage of blood to the hepatic vein and of gall through the bile duct system. Like other parallel organised organs, the liver has a pronounced volume effect. Radiation induced liver disease (RILD), which primarily reflects a veno-occlusive phenomenon [50,51], has been observed in 5% of patients receiving whole-liver doses of 30–35 Gy in 2

Gy fractions [52–54] and the TD_{50} values for patients receiving whole liver irradiation for liver metastases and for primary hepatobiliary cancer were estimated to be around 46 Gy and 40 Gy respectively [55].

Since normal liver radiation damage is one of the major limiting factors in radiotherapy of the liver, methods for measurement of liver function – and specifically for determining the spatial distribution of liver function – have specific relevance. These methods may potentially be useful in selection of patients for radiotherapy, for determination of radiation damage in treated patients, for adaptive strategies during therapy and most importantly by integration into radiotherapy planning.

Blood clearance of galactose and indocyanine green are established methods for evaluation of the total liver metabolism [56,57]. Both substances are almost exclusively removed from circulation by the hepatocytes and following IV injection of one of the substances, the total hepatic capacity can be estimated from serum values of consecutive blood samples.

Conventional and dynamic contrast-enhanced CT-scanning

Radiation-induced reaction of the liver is characterised by hypodense changes visible in non-contrast-enhanced as well as in contrast enhanced-conventional CT. In a study of 36 patients treated by SBRT for hepatic tumours in Heidelberg, 74% of patients demonstrated a hypodense reaction on non-enhanced CT in irradiated liver one to five months after receiving doses above a threshold of 14 Gy. Three distinct patterns of reaction were identified by the contrast enhanced CT, depending on density characteristics (hypo-, iso- or hyperdense reaction) in the portal, venous and late contrast phases.

Dynamic contrast-enhanced CT (DCE-CT) has been used for functional imaging of the liver by Cao et al. from Ann Arbor [58–60]. In DCE-CT an extended cine series of images are acquired over a period of 120 seconds using a multi-slice CT scanner after bolus injection of IV contrast medium. Hepatic perfusion can be estimated from time changes in Hounsfield units (HU) of the artery, portal vein, and hepatic parenchyma compartments, respectively. Images showing the spatial distribution of perfusion can be overlaid on the CT scan resulting in a 3D illustration of hepatic perfusion. Technical constraints currently limit the technique to viewing a limited size slice of the liver at a time. The Ann Arbor group investigated portal vein perfusion in ten patients treated with conformal RT with doses between 48 Gy and 78 Gy in 1.5 Gy fractions for a variety of different tumours in the liver. DCE-CT was performed prior to radiotherapy, then after 15 and

30 fractions respectively. They found that regional portal vein perfusion was significantly reduced in irradiated liver, most pronounced at one month after treatment, and that the reduction correlated with radiation dose [60]. In a subsequent modelling study of 11 patients, the group found undetectable portal vein perfusion in irradiated liver volumes ranging from 0 to 39%, dependent on the dose distribution. This study also demonstrated significant correlation between mean portal perfusion and functional capacity of the liver measured by indocyanine green clearance.

Diffusion weighted MRI

Diffusion weighted (DW)-MRI explores the random motion of water molecules in tissue. Movement of water molecules in biological tissues is restricted by interactions with cell membranes and macromolecules. Cellular density and variability are among the factors determining the DW-MRI signal of a tissue. At the Princess Margaret Hospital, tumour response and normal tissue injury was studied in 11 patients receiving hypofractionated RT for liver tumours [61]. This study primarily aimed at investigating time changes in diffusion in tumour tissue, but results for liver were also reported. In a preliminary analysis of the study, the population-average apparent diffusion coefficients (ADC) in liver tissue receiving a radiation dose higher than 8 Gy dropped during treatment and follow-up. This change was relatively small, but significant.

SPECT and SPECT/CT

SPECT scanning with ^{99m}Tc imino-diacetic acid (^{99m}Tc -HIDA) or cholescintigraphy is an established method for detection of disorders of the bile duct system. Dynamic and static ^{99m}Tc -HIDA SPECT may provide information on the functional status of the liver [62]. So far, use of HIDA scans has primarily been reported in studies of bile duct disorders such as primary sclerosing cholangitis. However, combined with CT this method may potentially be useful for treatment planning in radiotherapy of liver tumors.

Hepatic functional reserve was evaluated using sequential ^{99m}Tc -galactosyl human serum albumin (^{99m}Tc -GSA) SPECT in a small Japanese study of three patients receiving proton therapy for hepatic malignancies [63]. Using contrast-enhanced CT scans, the high dose volume appeared hypodense and scintigraphy consistently revealed focal depression of ^{99m}Tc -GSA uptake in these volumes. Some of these changes remained for one year.

Mebrofenin is an iminodiacetic acid that enters the hepatocyte, traverses to the bile canaliculi and it

is excreted with the bile. By IV infusion of technetium-labelled mebrofenin (^{99m}Tc -Mebrofenin) and SPECT/CT, the spatial distribution of hepatic metabolism can be determined. So far, the experience based on this method is limited to patients undergoing surgical resection, where the method accurately predicted the residual liver following the resection [64,65]. However, the method may be useful for determining the volume of functional liver for treatment planning of liver tumours.

PET/CT

Positron labelled 2-[^{18}F]fluoro-2-deoxygalactose (FDGal) PET/CT scanning has recently been developed for 3D determination of liver metabolism. The kinetics of up-take and elimination of galactose in the liver has been studied by dynamic PET/CT in a pig model, where the technique delivered high-resolution spatial information on local metabolism of the liver [66]. A study on PET/CT in patients undergoing hypofractionated SBRT for liver tumours is ongoing at Aarhus University Hospital. The method may therefore be useful in prediction of RILD and in planning of RT for liver tumours.

Summary

RT for liver tumours is being offered with increasing frequency and with the liver as the most important organ at risk there is a great demand for functional imaging of the liver. Several imaging modalities offer information on the spatial distribution of the liver function. So far, all these methods have shown that the spatial distribution of liver function is heterogeneous, which is clearly of crucial importance when considering the use of functional imaging in radiotherapy planning. It remains to be shown whether the spatial distribution of liver function is constant with time.

Portal vein perfusion measured by DCE-CT is currently the most established measure of spatial liver function. It represents a surrogate of hepatic function, but a correlation has been demonstrated between perfusion and function. There are suitable tracers available for SPECT-based methods, but SPECT is hampered by relatively poor spatial resolution. Novel methods based on MRI and PET/CT are promising, however, they have been studied only to a limited extent. Functional imaging of the liver is still considered investigational and further clinical study is warranted.

Imaging of salivary gland function

Radiation-induced loss of salivary gland function leads to dryness of mouth (xerostomia), which is a

distressing side-effect after RT for head and neck cancer, impacting on dental status, speech, swallowing, body weight and quality of life. The incidence and severity of parotid dysfunction appears to be related to the RT dose delivered, the percent of parotid volume irradiated, and the pre-irradiation parotid function.

Imaging techniques for salivary gland function measurements in RT are not yet on the shelf for routine use. The existing reports on parotid-sparing IMRT techniques have primarily used stimulated salivary flow measurements, where the saliva output is collected and measured, as an objective, specific endpoint in addition to questionnaires and toxicity scales. Saliva output collections, however, are not applicable to the submandibular glands, and they cannot assess function in sub-regions of the salivary glands. Thus, new volumetric imaging techniques should have a great potential as analytical measures in clinical trials, and potentially also in clinical routine. The recent QUANTEC review on salivary function [67] has shown good correlation between imaged and directly measured TD_{50} , although the imaged TD_{50} 's were generally higher than those directly measured. In the following, the existing data on salivary gland scintigraphy, SPECT (^{99m}Tc -pertechnetate), PET (^{11}C methionine), and functional MRI (DCE-MRI and DW-MRI) are presented.

Salivary gland scintigraphy and SPECT

The parotid glands may be imaged and their function assessed using ^{99m}Tc -pertechnetate [68]. Compared to flow measurements, these scans can supply additional information by following changes in the uptake and excretion function of the parotid glands.

Maes et al. [69] from Leuven University Hospital used salivary gland scintigraphy of 39 head and neck cancer patients to evaluate a 3D conformal parotid-sparing technique. They found a significant dose-response relationship between mean salivary excretion fraction (SEF) and mean parotid dose, but no correlation could be demonstrated between Visual Analogue Scale or LENT SOMA scores and the functional imaging of the parotids.

Van Acker et al. [70] from the same group investigated the utility of salivary gland scintigraphy combined with SPECT. Twenty-one patients with head and neck cancer were studied before and one month after RT with biplanar dynamic acquisition scintigraphy followed by SPECT before and after stimulation with carbachol. The SEF was calculated both from the geometric mean planar image for each parotid and from the SPECT data for each transverse plane through the parotids. The RT-induced changes in the SEF (dSEF) were correlated with radiation dose to the parotids. A linear correlation

was found between the dSEF calculated using SPECT and the radiation dose.

In a third paper from Leuven group, Bussels et al. [71] were the first to investigate individual slice-by-slice relationship between SPECT signal and RT dose. Sixteen head and neck cancer patients had a salivary scintigraphy combined with SPECT before and seven months after RT. The SEF after stimulation was measured in 8–12 selected SPECT slices of each parotid. Since the planning CT-scan and the SPECT-scintigraphy were performed in the same treatment position, the dose to a transverse slice within the parotid gland could be matched to the dSEF of that respective slice. Within individual parotid glands, the SEF's of the different slices were almost equal. Doses as low as 10–15 Gy could result in a serious loss of function. The mean dose resulting in 50% loss of salivary excretion fraction (D_{50}) seven months after RT was 22.5 Gy. A large inter-patient variability was found in D_{50} . The authors concluded that salivary SPECT is a useful tool for the evaluation of the salivary function of different slices within the parotid gland. The different slices within one parotid gland act as functional sub-units contributing equally to the function of the entire gland. The observation that low doses (10–15 Gy) could induce serious loss of function was recently confirmed by the QUANTEC review [67]. This low value is, however, not directly supported by flow data, where the threshold for clinical dysfunction generally is higher [72,73].

The largest series so far using SPECT was published by Roesink et al. from the University Medical Centre Utrecht in 2004 [74]. Ninety-six patients with primary or postoperative RT for various malignancies in the head-and-neck region were prospectively evaluated before RT, six weeks after RT, and one year after RT. CT-based treatment planning was used to derive dose–volume histograms of the parotid glands. The SEF decreased from 44 to 19% at six weeks after RT, but recovered to a SEF of 32% at one year after RT. The reduction in post-RT SEF correlated significantly with the mean parotid gland dose. The threshold dose for post-treatment SEF parotid ratio of <45% was found to be 29 Gy and 43 Gy at six weeks and one year after RT, respectively. The authors concluded that when direct flow measurements are not feasible, parotid scintigraphy appears to be a good indicator of gland function. The institutional series has recently been merged with experience from other centres and the pooled data has established a threshold dose of approximately 39 Gy [72].

PET

PET can be used for salivary gland function assessment due to the metabolic activity of the glands. PET

delivers very similar information to SPECT, i.e. volumetric images of gland metabolism, but with superior spatial resolution. For measuring protein synthesis, L-[methyl- ^{11}C] methionine (^{11}C -methionine) is a commonly used PET tracer. It has been tested for measuring liver protein synthesis and assessing excretory pancreas function. Furthermore, ^{11}C -methionine has been tested for imaging response of head and neck cancer to RT [75], where it was noted that salivary gland uptake of ^{11}C -methionine decreased after RT. Based on these findings, Buus et al. [76,77] from Aarhus University Hospital hypothesised that regional salivary gland function could be measured by dynamic ^{11}C -methionine PET, and that the PET measure of salivary gland function are reduced dependent on the radiation dose. A 3D voxel-by-voxel comparison of the radiation dose and parotid gland function in individual patients was used to establish the radiation dose response relationship of parotid and submandibular salivary glands. Twelve head and neck cancer patients were examined by dynamic ^{11}C -methionine PET after RT. The net metabolic clearance of ^{11}C -methionine of the parotid gland, K , was established as the primary analytic endpoint reflecting salivary gland function. Parametric images of the K were generated, co-registered and compared voxel-by-voxel with the 3D radiation dose plan within the parotid gland to assess the individual radiation dose–function relationship (Figure 5). In each patient, voxel-values of K decreased with increasing radiation dose. Population-based analysis showed a sigmoidal dose response relationship of parotid gland, from which a threshold radiation dose of 16 Gy was estimated, along with a mean TD_{50} of 30 Gy.

Overall, the current studies using SPECT or PET show comparable mean TD_{50} values. Both methods enable sub-organ comparison of the regional radiation dose with the regional parotid gland function. This is a potential advantage compared to parotid flow measurements, where only a single output measure of the entire gland excretion is produced.

MRI

Functional MRI has emerged as a promising new tool for imaging of characteristic changes resulting from RT, also in the salivary glands. Compared to SPECT and PET, MRI has excellent soft-tissue contrast and is without carcinogenic risk. Only a few studies have so far focused on post-RT salivary gland assessment.

Nomayr et al. [78] described the MRI changes in head and neck tissues observed in 52 patients after RT. For parotid glands they found that the glands decreased in volume by an average of 26% after

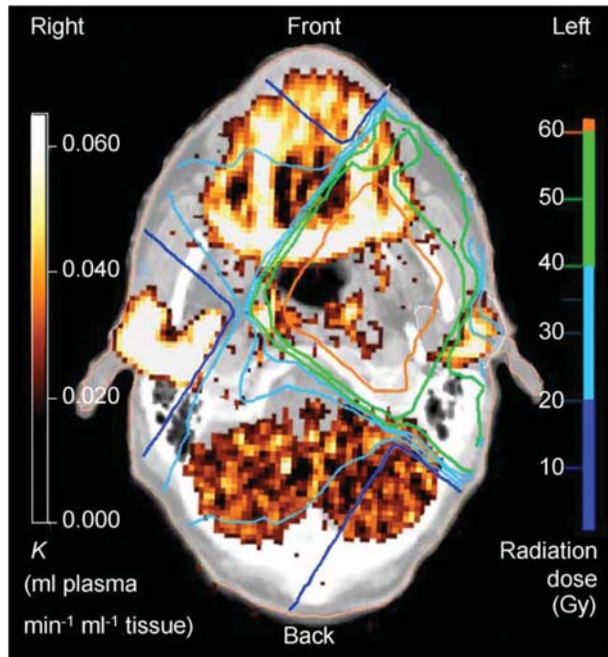


Figure 5. Transaxial co-registered image of the CT dose-plan and functional PET through the parotid glands. The CT dose-plan shows the radiation isodose curves (right-hand colour scale). The functional PET image gives voxel values of the net metabolic clearance of ^{11}C -methionine (left-hand colour scale). From Buus et al. [76].

30 Gy and 40% after 70 Gy. MR sialography with salivary secretion stimulation has been used to study post-irradiation changes in the salivary ducts in small patient series [79,80]. The authors conclude that 3D MR sialography is a promising approach for investigating xerostomia, because radiation-induced changes to the saliva content of the ducts can be visualised.

In a study with 21 patients with radiation-induced salivary gland injury, Zhang et al. [81] found that decreased salivary gland ADC values from intra-voxel incoherent motion echo-planar MRI correlated with decreased salivary function measured by scintigraphy. The correlation was weak, but still significant ($r = 0.36$, $p < 0.001$). They concluded that measurements of ADC on MRI might provide a non-invasive means of evaluating the functional status of the salivary gland, but more studies are needed before this method can be applied in the evaluation of salivary function in individual patients.

Dirix et al. performed diffusion-weighted MRI (DW-MRI) of the salivary glands in eight patients with head and neck cancer before and after parotid-sparing RT [82]. The baseline ADC value at rest was significantly higher after RT than before RT in the non-spared salivary glands but not in the spared parotid glands. In the contralateral parotid glands, the same response was seen as before RT. This pattern was completely lost in the non-spared glands. These results corresponded with preservation or loss

of salivary function, respectively, as confirmed by salivary gland scintigraphy. The data suggest that DW-MRI may be a useful tool for non-invasive evaluation of functional changes in the major salivary glands after RT.

The merits of dynamic contrast-enhanced MRI (DCE-MRI) have recently been studied by Juan et al. [83]. Parotid perfusion after irradiation based on a two-compartment tracer kinetic model was studied in 19 head and neck patients treated with RT and 19 matched controls. Perfusion parameters of the parotid glands were analysed based on the Brix model from T1-weighted DCE-MRI. The irradiated parotid glands showed dose-dependent perfusion changes, suggesting that quantitative DCE-MRI is a potential tool for investigating parotid gland perfusion changes after RT.

There is still a long way to go before the exact role of functional MRI in salivary gland assessment is established. Larger clinical studies are needed, comparing the MRI findings with the gold standards of stimulated saliva output, as well as scintigraphy and SPECT/PET.

Summary

Assessment of salivary gland function and its clinical consequences is important for head and neck RT trials, especially those focusing on xerostomia reduction. Although the current studies – with the modest numbers of patients included – generally lack a correlation with clinical and subjective xerostomia-related endpoints; functional imaging seems to be valuable for clinical radiobiology research and should be further studied and validated against other analytical tests.

Discussion

In the previous three sections, we have shown published accounts that clearly demonstrate that functional imaging can be used to preferentially avoid normal tissues not easily identifiable on solely anatomical images and that such imaging is a potentially very powerful tool for the early detection of radiotherapy-induced normal tissue injury. However, it is probably fair to say that, in this fast developing field, the full potential of functional imaging biomarkers of radiation-induced adverse effects has not been fully explored. It is hoped that improvement in the understanding of the basic mechanisms underlying the onset, dynamics and resolution of RT-induced injury will enable development of more specific functional imaging biomarkers [5] that will in turn be useful surrogates for clinically relevant outcomes. It should also be borne in mind that temporal variations

in normal tissue function, rather than the functional status at a single pre- or post-RT time point, may give additional useful information that will allow us to exploit the full potential of biological image-guided radiotherapy [84].

A strong case for the routine use of FDG PET for target volume delineation has been made for NSCLC [85], with other indications having more limited supporting evidence being cautiously recommended. In making these recommendations, it is emphasised that incorporation of functional imaging into RT planning is technically challenging. The lessons learned from target volume delineation are equally valid for defining normal tissues: the need for rigorous quality assurance procedures and data acquisition protocols and an understanding of the inherent uncertainty in the functional data is crucially important [86,87] (e.g. limited spatial resolution, quantitative accuracy, temporal stability and the challenge of validation). Similar attention to detail is required when generating contours from the functional data. Rigorous protocols using predefined window levels and colour settings need to be developed and quality controlled using phantom measurements. Although much work has been reported describing threshold or target-to-background based automatic segmentation tools, most are not adequate for unsupervised clinical use [88]. The best available method to date for PET/CT is visual contouring by a radiation oncologist in cooperation with a nuclear medicine specialist, following a well-defined protocol [89].

It remains challenging to accurately co-register a planning CT scan with a typically low spatial resolution functional data set containing very little rigid anatomical information. For example, in the lung an obvious solution is to use a hybrid SPECT/CT scanner, either to produce the RT planning CT directly, or to allow CT/CT fusion (for MRI, a T_1 or T_2 anatomical image could be acquired without moving the patient to allow registration of the hyperpolarised ^3He data). In the absence of a hybrid scanner, marker-based registration is a practical option. Multimodality markers that are visible on CT (hyper-dense ring) and SPECT (^{57}Co) are commercially available and easy to use; with the proviso that the patient has their CT and SPECT in quick succession without removing the markers [24]. If care is taken to use identical immobilisation equipment on both scanners, registration should be limited to rigid body translations only. For lung imaging, ideally a mid-phase CT would be used to achieve the best quality registration with SPECT, which is acquired during free-breathing. However, it is worth bearing in mind that the SPECT data are of most use in the presence of large focal perfusion deficits and therefore affect the choice of gross beam direction; also the lack of high spatial frequency

information in the SPECT data mean that aiming for sub-millimetre co-registration may be unrealistic.

Recent work from the Vancouver Cancer Centre, Canada, investigating the use of non-rigid registration methods for SPECT-guided lung RT have shown that non-rigid methods can provide a higher degree of accuracy than rigid methods, but in some cases the irregular deformation fields produced would preclude their use in RT [90]. In the liver, extensive studies using fluoroscopy, 4D-CT and cine-MRI have shown that regular breathing can result in liver displacements ≥ 2 cm with significant elastic deformation [6]. Non-rigid registration methods have been successfully applied to liver imaging using a constrained biomechanical deformation model based on population data and a “navigator channel” from 4D-CT [91]. The navigator channel is a quasi-1D region of interest placed on the liver boundary. Changes in intensity in this channel are used to select the appropriate breathing phase in the model. A number of techniques have been demonstrated for adaptive RT in the liver, ranging in complexity from breath-hold to real-time tracking. The need for image guidance – and registration of the localisation image with an appropriate reference image – is a common feature of all techniques [92]. There is clearly scope for further work developing and validating non-rigid image registration methods for functional image-guided RT.

Future studies and applications

In the sections above, we have reviewed the possible uses of functional imaging of normal tissues in RT, focussing on applications in the lung, liver and the parotids. The applications fall into two main groups: those that seek to avoid well-functioning normal tissues and those that seek to predict or model normal tissue response to RT. In this section we will briefly discuss the potential future strategies that might be explored with these two groups.

Normal tissue avoidance

It is clear that in functionally heterogeneous organs, information on the spatial distribution of function could be of real benefit to RT planning. Depending on the geometrical relationships between the target and functioning normal tissues, a number of possible planning strategies have been demonstrated:

1. The use of fused functional images and planning CT as a visual guide to beam placement and beam shaping.
2. The calculation of “functional” dose-volume metrics, such as fDVHs to compare rival plans.

3. The use of functional image data to directly drive inverse plan optimisation, either by segmenting “functional organs at risk” or using individual functional voxel values, i.e. the normal tissue correspondence to the dose painting-by-numbers (DPBN) concept.

The technical feasibility of DPBN or contour-based target segmentation using functional images has been clearly demonstrated [93–96] in recent years. The fact that DPBN and contour-based approaches have been shown to be relatively robust to inherent uncertainties in the functional data [87] and that the optimum number of different prescription dose levels is small [97] suggest that the extension of this concept to include functional maps of normal tissues as well as tumours should be feasible. Added to this, the recent advances in RT beam delivery using intensity-modulated arcs increase the degrees of freedom available to the treatment planner, making the search-space available for normal tissue avoidance even larger.

Toxicity modelling

It has been shown that three-dimensional features of a dose distribution are important predictors of RT outcomes [98]. Models which explicitly include these three-dimensional features have been shown to outperform simple DVH-based models [99]. For normal tissues that exhibit heterogeneous baseline patterns of function, incorporation of the local functional status and local dose into a predictive model should further improve performance. Examples of this to date include the use of mean perfusion-weighted lung dose as opposed to simple mean lung dose for predicting radiation pneumonitis in the lung (see section 3). One of the major challenges to building such models is that, to date, there are very little data available with combined images of normal function, 3D delivered radiation dose and clinical outcomes using established morbidity scores. The adoption of a “data-pooling culture” as suggested in the recent QUANTEC vision paper [100] where consistent and high-quality data would be collected in central repositories would be enormously helpful for building and validating useful “functional NTCP” models, with applications including:

1. Pre-treatment assessment of potential treatment-related toxicity, which could be used for patient selection.
2. Optimisation of treatment plans using fNTCP-based constraints.
3. Patient-specific dose escalation using iso-fNTCP constraints.

Clinical studies are in progress in a number of centres collecting such data, but more are clearly required.

Conclusion

Published results to date demonstrate the clinical feasibility of using functional imaging in RT planning to preferentially avoid normal tissues not easily identifiable on solely anatomical images. Statistically significant reductions in dose to functioning lung have been shown for the small percentage of NSCLC patients with large focal perfusion deficits and the use of IMRT also shown to further improve dose distributions. However, further work is required to establish a link between changes in apparent perfusion on imaging and clinically relevant measures of pulmonary function. In the liver, several different imaging modalities offer information about the spatial distribution of function which may potentially be useful for treatment planning and post-treatment imaging may be useful for early detection of radiation-induced reactions. In the head and neck assessment of salivary gland function has been shown to be important, especially for RT trials focusing on xerostomia reduction. Functional imaging of salivary gland function seems to be valuable for clinical radiobiology research and should be further studied and validated against other analytical tests.

For all of the techniques reviewed however, further research is required to better understand the link between imaging data and relevant clinical endpoints. Prospective data collection through well-constructed studies using established morbidity scores is clearly a priority if significant progress is to be made in this area.

Acknowledgements

M. Partridge acknowledges NHS funding from the NIHR Biomedical Research Centre and funding from CR UK under grant C46/A10588. T. Yamamoto is grateful to Dr. Paul J. Keall at Stanford University for reviewing the paragraphs on 4D-CT ventilation imaging in Section 3 (Imaging of lung function) and providing helpful suggestions. Morten Høyer is supported by A.P. Moller and Chastine Mc-Kinney Møller Foundation. This work was supported by CIRRO – The Lundbeck Foundation Center for Interventional Research in Radiation Oncology, The Danish Council for Strategic Research and by research grants from the Danish Cancer Society and The Danish Council for Independent Research (FSS).

Declaration of interest: The authors report no conflicts of interest. The authors alone are responsible for the content and writing of the paper.

References

- [1] Ling CC, Humm J, Larson S, Amols H, Fuks Z, Leibel S, et al. Towards multidimensional radiotherapy (MD-CRT): Biological imaging and biological conformality. *Int J Radiat Oncol Biol Phys* 2000;47:551–60.
- [2] Grau C, Muren LP, Hoyer M, Lindegaard J, Overgaard J. Image-guided adaptive radiotherapy – integration of biology and technology to improve clinical outcome. *Acta Oncol* 2008;47:1182–5.
- [3] Greco C, Clifton Ling C. Broadening the scope of image-guided radiotherapy (IGRT). *Acta Oncol* 2008;47:1193–200.
- [4] Hanahan D, Weinberg RA. The hallmarks of cancer. *Cell* 2000;100:57–70.
- [5] Jeraj R, Cao Y, Ten Haken RK, Hahn C, Marks L. Imaging for assessment of radiation-induced normal tissue effects. *Int J Radiat Oncol Biol Phys* 2010;76:S140–4.
- [6] Pan CC, Kavanagh BD, Dawson LA, Li XA, Das SK, Miften M, et al. Radiation-associated liver injury. *Int J Radiat Oncol Biol Phys* 2010;76:S94–100.
- [7] Sundgren PC, Cao Y. Brain irradiation: Effects on normal brain parenchyma and radiation injury. *Neuroimaging Clin N Am* 2009;19:657–68.
- [8] Evans ES, Hahn CA, Kocak Z, Zhou SM, Marks LB. The role of functional imaging in the diagnosis and management of late normal tissue injury. *Semin Radiat Oncol* 2007;17:72–80.
- [9] Franiel T, Ludemann L, Taupitz M, Bohmer D, Beyersdorff D. MRI before and after external beam intensity-modulated radiotherapy of patients with prostate cancer: The feasibility of monitoring of radiation-induced tissue changes using a dynamic contrast-enhanced inversion-prepared dual-contrast gradient echo sequence. *Radiother Oncol* 2009;93:241–5.
- [10] Kershaw LE, Logue JP, Hutchinson CE, Clarke NW, Buckley DL. Late tissue effects following radiotherapy and neoadjuvant hormone therapy of the prostate measured with quantitative magnetic resonance imaging. *Radiother Oncol* 2008;88:127–34.
- [11] Russell NS, Hoving S, Heeneman S, Hage JJ, Woerdeman LA, de Bree R, et al. Novel insights into pathological changes in muscular arteries of radiotherapy patients. *Radiother Oncol* 2009;92:477–83.
- [12] Marks LB, Munley MT, Bentel GC, Zhou SM, Hollis D, Scarfone C, et al. Physical and biological predictors of changes in whole-lung function following thoracic irradiation. *Int J Radiat Oncol Biol Phys* 1997;39:563–70.
- [13] Otto K. Volumetric modulated arc therapy: IMRT in a single gantry arc. *Med Phys* 2008;35:310–7.
- [14] Nioutsikou E, Partridge M, Bedford JL, Webb S. Prediction of radiation-induced normal tissue complications in radiotherapy using functional image data. *Phys Med Biol* 2005;50:1035–46.
- [15] Ricardi U, Filippi AR, Guarneri A, Giglioli FR, Mantovani C, Fiandra C, et al. Dosimetric predictors of radiation-induced lung injury in stereotactic body radiation therapy. *Acta Oncol* 2009;48:571–7.
- [16] Marks LB, Spencer DP, Bentel GC, Ray SK, Sherouse GW, Sontag MR, et al. The utility of SPECT lung perfusion scans in minimizing and assessing the physiologic consequences of thoracic irradiation. *Int J Radiat Oncol Biol Phys* 1993;26:659–68.
- [17] Lu Y, Spelbring DR, Chen GT. Functional dose-volume histograms for functionally heterogeneous normal organs. *Phys Med Biol* 1997;42:345–56.
- [18] Kutcher GJ, Burman C, Brewster L, Goitein M, Mohan R. Histogram reduction method for calculating complication probabilities for three-dimensional treatment planning evaluations. *Int J Radiat Oncol Biol Phys* 1991;21:137–46.
- [19] Niemierko A, Goitein M. Modeling of normal tissue response to radiation: The critical volume model. *Int J Radiat Oncol Biol Phys* 1993;25:135–45.
- [20] Kwa SL, Theuvs JC, Wagenaar A, Damen EM, Boersma LJ, Baas P, et al. Evaluation of two dose-volume histogram reduction models for the prediction of radiation pneumonitis. *Radiother Oncol* 1998;48:61–9.
- [21] Lyman JT. Complication probability as assessed from dose-volume histograms. *Radiat Res Suppl* 1985;8:S13–9.
- [22] Munley MT, Marks LB, Scarfone C, Sibley GS, Patz EF, Jr., Turkington TG, et al. Multimodality nuclear medicine imaging in three-dimensional radiation treatment planning for lung cancer: Challenges and prospects. *Lung Cancer* 1999;23:105–14.
- [23] Seppenwoolde Y, Engelsman M, De Jaeger K, Muller SH, Baas P, McShan DL, et al. Optimizing radiation treatment plans for lung cancer using lung perfusion information. *Radiother Oncol* 2002;63:165–77.
- [24] Christian JA, Partridge M, Nioutsikou E, Cook G, McNair HA, Cronin B, et al. The incorporation of SPECT functional lung imaging into inverse radiotherapy planning for non-small cell lung cancer. *Radiother Oncol* 2005;77:271–7.
- [25] McGuire SM, Zhou S, Marks LB, Dewhurst M, Yin FF, Das SK. A methodology for using SPECT to reduce intensity-modulated radiation therapy (IMRT) dose to functioning lung. *Int J Radiat Oncol Biol Phys* 2006;66:1543–52.
- [26] Lavrenkov K, Christian JA, Partridge M, Nioutsikou E, Cook G, Parker M, et al. A potential to reduce pulmonary toxicity: The use of perfusion SPECT with IMRT for functional lung avoidance in radiotherapy of non-small cell lung cancer. *Radiother Oncol* 2007;83:156–62.
- [27] Lavrenkov K, Singh S, Christian JA, Partridge M, Nioutsikou E, Cook G, et al. Effective avoidance of a functional spect-perfused lung using intensity modulated radiotherapy (IMRT) for non-small cell lung cancer (NSCLC): An update of a planning study. *Radiother Oncol* 2009;91:349–52.
- [28] van Luijk P, Novakova-Jiresova A, Faber H, Steneker MN, Kampinga HH, Meertens H, et al. Relation between radiation-induced whole lung functional loss and regional structural changes in partial irradiated rat lung. *Int J Radiat Oncol Biol Phys* 2006;64:1495–502.
- [29] Ma J, Zhang J, Zhou S, Hubbs JL, Foltz RJ, Hollis DR, et al. Association between RT-induced changes in lung tissue density and global lung function. *Int J Radiat Oncol Biol Phys* 2009;74:781–9.
- [30] Zhang J, Ma J, Zhou S, Hubbs JL, Wong TZ, Foltz RJ, et al. Radiation-induced reductions in regional lung perfusion: 0.1–12 year data from a prospective clinical study. *Int J Radiat Oncol Biol Phys* 2010;76:425–32.
- [31] Ireland RH, Bragg CM, McJury M, Woodhouse N, Fichelle S, van Beek EJ, et al. Feasibility of image registration and intensity-modulated radiotherapy planning with hyperpolarized helium-3 magnetic resonance imaging for non-small-cell lung cancer. *Int J Radiat Oncol Biol Phys* 2007;68:273–81.
- [32] Bates EL, Bragg CM, Wild JM, Hatton MQ, Ireland RH. Functional image-based radiotherapy planning for non-small cell lung cancer: A simulation study. *Radiother Oncol* 2009;93:32–6.
- [33] Ireland RH, Woodhouse N, Hoggard N, Swinscoe JA, Foran BH, Hatton MQ, et al. An image acquisition and registration strategy for the fusion of hyperpolarized helium-3 MRI and x-ray CT images of the lung. *Phys Med Biol* 2008;53:6055–63.
- [34] Guerrero T, Sanders K, Noyola-Martinez J, Castillo E, Zhang Y, Tapia R, et al. Quantification of regional ventilation from treatment planning CT. *Int J Radiat Oncol Biol Phys* 2005;62:630–4.

- [35] Simon BA. Non-invasive imaging of regional lung function using x-ray computed tomography. *J Clin Monit Comput* 2000;16:433–42.
- [36] Guerrero T, Sanders K, Castillo E, Zhang Y, Bidaut L, Pan T, et al. Dynamic ventilation imaging from four-dimensional computed tomography. *Phys Med Biol* 2006;51:777–91.
- [37] Yaremko BP, Guerrero TM, Noyola-Martinez J, Guerra R, Lege DG, Nguyen LT, et al. Reduction of normal lung irradiation in locally advanced non-small-cell lung cancer patients, using ventilation images for functional avoidance. *Int J Radiat Oncol Biol Phys* 2007;68:562–71.
- [38] Reinhardt JM, Ding K, Cao K, Christensen GE, Hoffman EA, Bodas SV. Registration-based estimates of local lung tissue expansion compared to xenon CT measures of specific ventilation. *Med Image Anal* 2008;12:752–63.
- [39] Zhong H, Fragoso M, Patel S, Ajlouni M, Movsas B, Chetty I. A method to evaluate region-specific pulmonary function using 4D CT images for lung cancer patients undergoing radiation therapy. *Med Phys* 2009;36:2762 (Abstract).
- [40] Yamamoto T, Kabus S, von Berg J, Lorenz C, Keall PJ. Impact of four-dimensional computed tomography pulmonary ventilation imaging-based functional avoidance for lung cancer radiotherapy. *Int J Radiat Oncol Biol Phys* 2010;75 (suppl 1) S443 (abstract).
- [41] Yamamoto T, Kabus S, von Berg J, Klinder T, Blaffert T, Lorenz C, et al. Physiological validation of 4D-CT-based ventilation imaging in patients with chronic obstructive pulmonary disease (COPD). *Med Phys* 2009;36:2821 (Abstract).
- [42] Kabus S, von Berg J, Yamamoto T, Opfer R, Keall PJ. Lung ventilation estimation based on 4D-CT imaging. Proceedings of the First International Workshop on Pulmonary Image Analysis, MICCAI 2008. 2008;73–81.
- [43] Rogalla P, Rogalla N, Schmidt B, Hamm B, Lambcke A, Hein P. Respiratory gated chest CT in pulmonary compromised patients: Correlation with lung function tests. Proceedings of ERC 2008. 2008;297 (Abstract).
- [44] Vik T, Kabus S, von Berg J, Ens K, Dries S, Klinder T, et al. Validation and comparison of registration methods for free-breathing 4D lung CT. In: Reinhardt JM, Pluim JPW, editors. Proceedings of SPIE Medical Imaging: SPIE. 2008; 69142P-69141-69142P-69110.
- [45] Christensen GE, Song JH, Lu W, El Naqa I, Low DA. Tracking lung tissue motion and expansion/compression with inverse consistent image registration and spirometry. *Med Phys* 2007;34:2155–63.
- [46] von Berg J, Barschdorf H, Blaffert T, Kabus S, Lorenz C. Surface based cardiac and respiratory motion extraction for pulmonary structures from multi-phase CT. Proceedings of SPIE 2007. 2007;65110Y.
- [47] Weese J, Kaus M, Lorenz C, Lobregt S, Truyen R, Pekar V. Shape constrained deformable models for 3D medical image segmentation. In: Insana MF, Leahy RM, editors. Proceedings of IPMI 2001. 2001;380–7.
- [48] Divgi CR. Molecular imaging of pulmonary cancer and inflammation. *Proc Am Thorac Soc* 2009;6:464–8.
- [49] Stroian G, Martens C, Souhami L, Collins DL, Seuntjens J. Local correlation between Monte-Carlo dose and radiation-induced fibrosis in lung cancer patients. *Int J Radiat Oncol Biol Phys* 2008;70:921–30.
- [50] Reed GB, Jr., Cox AJ, Jr. The human liver after radiation injury. A form of veno-occlusive disease. *Am J Pathol* 1966; 48:597–611.
- [51] Lawrence TS, Robertson JM, Anscher MS, Jirtle RL, Ensminger WD, Fajardo LF. Hepatic toxicity resulting from cancer treatment. *Int J Radiat Oncol Biol Phys* 1995;31: 1237–48.
- [52] Austin-Seymour MM, Chen GT, Castro JR, Saunders WM, Pitluck S, Woodruff KH, et al. Dose volume histogram analysis of liver radiation tolerance. *Int J Radiat Oncol Biol Phys* 1986;12:31–5.
- [53] Wharton JT, Delclos L, Gallager S, Smith JP. Radiation hepatitis induced by abdominal irradiation with the cobalt 60 moving strip technique. *Am J Roentgenol Radium Ther Nucl Med* 1973;117:73–80.
- [54] Ingold JA, Reed GB, Kaplan HS, Bagshaw MA. Radiation hepatitis. *Am J Roentgenol Radium Ther Nucl Med* 1965; 93:200–8.
- [55] Dawson LA, Ten Haken RK. Partial volume tolerance of the liver to radiation. *Semin Radiat Oncol* 2005;15:279–83.
- [56] Gottlieb ME, Stratton HH, Newell JC, Shah DM. Indocyanine green. Its use as an early indicator of hepatic dysfunction following injury in man. *Arch Surg* 1984;119:264–8.
- [57] Tygstrup N. Determination of the hepatic elimination capacity (L_m) of galactose by single injection. *Scand J Clin Lab Invest Suppl* 1966;18:118–25.
- [58] Cao Y, Alspaugh J, Shen Z, Balter JM, Lawrence TS, Ten Haken RK. A practical approach for quantitative estimates of voxel-by-voxel liver perfusion using DCE imaging and a compartmental model. *Med Phys* 2006;33:3057–62.
- [59] Cao Y, Pan C, Balter JM, Platt JF, Francis IR, Knol JA, et al. Liver function after irradiation based on computed tomographic portal vein perfusion imaging. *Int J Radiat Oncol Biol Phys* 2008;70:154–60.
- [60] Cao Y, Platt JF, Francis IR, Balter JM, Pan C, Normolle D, et al. The prediction of radiation-induced liver dysfunction using a local dose and regional venous perfusion model. *Med Phys* 2007;34:604–12.
- [61] Eccles CL, Haider EA, Haider MA, Fung S, Lockwood G, Dawson LA. Change in diffusion weighted MRI during liver cancer radiotherapy: Preliminary observations. *Acta Oncol* 2009;48:1034–43.
- [62] Jonas E, Hultcrantz R, Slezak P, Blomqvist L, Schnell PO, Jacobsson H. Dynamic (99m)Tc-HIDA SPET: Non-invasive measuring of intrahepatic bile flow. Description of the method and a study in primary sclerosing cholangitis. *Nucl Med Commun* 2001;22:127–34.
- [63] Igaki H, Tokuyue K, Takeda T, Sugahara S, Hata M, Hashimoto T, et al. Sequential evaluation of hepatic functional reserve by 99mTechnetium-galactosyl human serum albumin scintigraphy after proton beam therapy: A report of three cases and a review of the literatures. *Acta Oncol* 2006;45:1102–7.
- [64] de Graaf W, van Lienden KP, van Gulik TM, Bennink RJ. (99m)Tc-mebrofenin hepatobiliary scintigraphy with SPECT for the assessment of hepatic function and liver functional volume before partial hepatectomy. *J Nucl Med* 2010;51:229–36.
- [65] de Graaf W, Vetelainen RL, de Bruin K, van Vliet AK, van Gulik TM, Bennink RJ. 99mTc-GSA scintigraphy with SPECT for assessment of hepatic function and functional volume during liver regeneration in a rat model of partial hepatectomy. *J Nucl Med* 2008;49:122–8.
- [66] Sorensen M, Munk OL, Mortensen FV, Olsen AK, Bender D, Bass L, et al. Hepatic uptake and metabolism of galactose can be quantified in vivo by 2-[18F]fluoro-2-deoxygalactose positron emission tomography. *Am J Physiol Gastrointest Liver Physiol* 2008;295:G27–G36.
- [67] Deasy JO, Moiseenko V, Marks L, Chao KS, Nam J, Eisbruch A. Radiotherapy dose-volume effects on salivary gland function. *Int J Radiat Oncol Biol Phys* 2010;76:S58–63.
- [68] Rudat V, Munter M, Rades D, Grotz KA, Bajrovic A, Haberkorn U, et al. The effect of amifostine or IMRT to preserve the parotid function after radiotherapy of the head and neck region measured by quantitative salivary gland scintigraphy. *Radiother Oncol* 2008;89:71–80.

- [69] Maes A, Weltens C, Flamen P, Lambin P, Bogaerts R, Liu X, et al. Preservation of parotid function with uncomplicated conformal radiotherapy. *Radiother Oncol* 2002;63:203–11.
- [70] van Acker F, Flamen P, Lambin P, Maes A, Kutcher GJ, Weltens C, et al. The utility of SPECT in determining the relationship between radiation dose and salivary gland dysfunction after radiotherapy. *Nucl Med Commun* 2001;22:225–31.
- [71] Bussels B, Maes A, Flamen P, Lambin P, Erven K, Hermans R, et al. Dose-response relationships within the parotid gland after radiotherapy for head and neck cancer. *Radiother Oncol* 2004;73:297–306.
- [72] Houweling AC, Philippens ME, Dijkema T, Roesink JM, Terhaard CH, Schilstra C, et al. A comparison of dose-response models for the parotid gland in a large group of head-and-neck cancer patients. *Int J Radiat Oncol Biol Phys* 2010;76:1259–65.
- [73] Eisbruch A, Ten Haken RK, Kim HM, Marsh LH, Ship JA. Dose, volume, and function relationships in parotid salivary glands following conformal and intensity-modulated irradiation of head and neck cancer. *Int J Radiat Oncol Biol Phys* 1999;45:577–87.
- [74] Roesink JM, Moerland MA, Hoekstra A, Van Rijk PP, Terhaard CH. Scintigraphic assessment of early and late parotid gland function after radiotherapy for head-and-neck cancer: A prospective study of dose-volume response relationships. *Int J Radiat Oncol Biol Phys* 2004;58:1451–60.
- [75] Lindholm P, Leskinen-Kallio S, Grenman R, Lehtikoinen P, Nagren K, Teras M, et al. Evaluation of response to radiotherapy in head and neck cancer by positron emission tomography and [¹¹C]methionine. *Int J Radiat Oncol Biol Phys* 1995;32:787–94.
- [76] Buus S, Grau C, Munk OL, Bender D, Jensen K, Keiding S. ¹¹C-methionine PET, a novel method for measuring regional salivary gland function after radiotherapy of head and neck cancer. *Radiother Oncol* 2004;73:289–96.
- [77] Buus S, Grau C, Munk OL, Rodell A, Jensen K, Mouridsen K, et al. Individual radiation response of parotid glands investigated by dynamic ¹¹C-methionine PET. *Radiother Oncol* 2006;78:262–9.
- [78] Nomayr A, Lell M, Sweeney R, Bautz W, Lukas P. MRI appearance of radiation-induced changes of normal cervical tissues. *Eur Radiol* 2001;11:1807–17.
- [79] Astreimidou E, Roesink JM, Raaijmakers CP, Bartels LW, Witkamp TD, Lagendijk JJ, et al. 3D MR sialography as a tool to investigate radiation-induced xerostomia: Feasibility study. *Int J Radiat Oncol Biol Phys* 2007;68:1310–9.
- [80] Wada A, Uchida N, Yokokawa M, Yoshizako T, Kitagaki H. Radiation-induced xerostomia: Objective evaluation of salivary gland injury using MR sialography. *AJNR Am J Neuroradiol* 2009;30:53–8.
- [81] Zhang L, Murata Y, Ishida R, Ohashi I, Yoshimura R, Shibuya H. Functional evaluation with intravoxel incoherent motion echo-planar MRI in irradiated salivary glands: A correlative study with salivary gland scintigraphy. *J Magn Reson Imaging* 2001;14:223–9.
- [82] Dirix P, De Keyser F, Vandecaveye V, Stroobants S, Hermans R, Nuyts S. Diffusion-weighted magnetic resonance imaging to evaluate major salivary gland function before and after radiotherapy. *Int J Radiat Oncol Biol Phys* 2008;71:1365–71.
- [83] Juan CJ, Chen CY, Jen YM, Liu HS, Liu YJ, Hsueh CJ, et al. Perfusion characteristics of late radiation injury of parotid glands: Quantitative evaluation with dynamic contrast-enhanced MRI. *Eur Radiol* 2009;19:94–102.
- [84] Sovik A, Malinen E, Olsen DR. Adapting biological feedback in radiotherapy. *Semin Radiat Oncol* 2010;20:138–46.
- [85] MacManus M, Nestle U, Rosenzweig KE, Carrio I, Messa C, Belohlavek O, et al. Use of PET and PET/CT for radiation therapy planning: IAEA expert report 2006–2007. *Radiother Oncol* 2009;91:85–94.
- [86] McCall KC, Barbee DL, Kissick MW, Jeraj R. PET imaging for the quantification of biologically heterogeneous tumours: Measuring the effect of relative position on image-based quantification of dose-painting targets. *Phys Med Biol* 2010;55:2789–806.
- [87] Perrin R, Evans PM, Webb S, Partridge M. The use of PET images for radiotherapy treatment planning: An error analysis using radiobiological endpoints. *Med Phys* 2010;37:516–31.
- [88] Gregoire V, Haustermans K, Geets X, Roels S, Lonneux M. PET-based treatment planning in radiotherapy: A new standard? *J Nucl Med* 2007;48(Suppl 1):68S–77S.
- [89] Nestle U, Kremp S, Grosu AL. Practical integration of [¹⁸F]-FDG-PET and PET-CT in the planning of radiotherapy for non-small cell lung cancer (NSCLC): The technical basis, ICRU-target volumes, problems, perspectives. *Radiother Oncol* 2006;81:209–25.
- [90] Yin LS, Tang L, Hamarneh G, Gill B, Celler A, Shcherbinin S, et al. Complexity and accuracy of image registration methods in SPECT-guided radiation therapy. *Phys Med Biol* 2010;55:237–46.
- [91] Nguyen TN, Moseley JL, Dawson LA, Jaffray DA, Brock KK. Adapting liver motion models using a navigator channel technique. *Med Phys* 2009;36:1061–73.
- [92] Brock KK, Dawson LA. Adaptive management of liver cancer radiotherapy. *Semin Radiat Oncol* 2010;20:107–15.
- [93] Yang Y, Xing L. Towards biologically conformal radiation therapy (BCRT): Selective IMRT dose escalation under the guidance of spatial biology distribution. *Med Phys* 2005;32:1473–84.
- [94] Thorwarth D, Eschmann SM, Paulsen F, Alber M. Hypoxia dose painting by numbers: A planning study. *Int J Radiat Oncol Biol Phys* 2007;68:291–300.
- [95] Bentzen SM. Theragnostic imaging for radiation oncology: Dose-painting by numbers. *Lancet Oncol* 2005;6:112–7.
- [96] South CP, Partridge M, Evans PM. A theoretical framework for prescribing radiotherapy dose distributions using patient-specific biological information. *Med Phys* 2008;35:4599–611.
- [97] South CP, Evans PM, Partridge M. Dose prescription complexity versus tumor control probability in biologically conformal radiotherapy. *Med Phys* 2009;36:4379–88.
- [98] Buettner F, Gulliford SL, Webb S, Sydes MR, Dearnaley DP, Partridge M. Assessing correlations between the spatial distribution of the dose to the rectal wall and late rectal toxicity after prostate radiotherapy: An analysis of data from the MRC RT01 trial (ISRCTN 47772397). *Phys Med Biol* 2009;54:6535–48.
- [99] Buettner F, Gulliford SL, Webb S, Partridge M. Using dose-surface maps to predict radiation-induced rectal bleeding: A neural network approach. *Phys Med Biol* 2009;54:5139–53.
- [100] Deasy JO, Bentzen SM, Jackson A, Ten Haken RK, Yorke ED, Constine LS, et al. Improving normal tissue complication probability models: The need to adopt a “data-pooling” culture. *Int J Radiat Oncol Biol Phys* 2010;76:S151–4.